Spectrochimica Acta Part B: Atomic Spectroscopy 177 (2021) 106104

Contents lists available at ScienceDirect

Spectrochimica Acta Part B: Atomic Spectroscopy

journal homepage: www.elsevier.com/locate/sab

Optimization of instrumental parameters for improving sensitivity of single particle inductively-coupled plasma mass spectrometry analysis of gold

Virva Kinnunen *, Siiri Perämäki, Rose Matilainen

Department of Chemistry, Chemistry in Circular Economy, University of Jyväskylä, P.O. Box 35, FI-40014 Jyväskylä, Finland

ARTICLE INFO

Keywords:
SpICP-MS
Instrumental parameters
Nanoparticles
Optimization
Matrix effect

ABSTRACT

Single particle inductively-coupled plasma mass spectrometry (spICP-MS) is a promising technique for analysis of engineered nanoparticles, whose utilization has increased substantially over the past years. Optimization of instrumental conditions is, however, crucial to improve the sensitivity and precision of nanoparticle (NP) detection. In this study, the influence of ICP-MS instrumental parameters (nebulizer gas flow, plasma radiofrequency-power and sampling depth) on the signal intensity of gold in spICP-MS was evaluated using dispersions of Au NPs and a solution of dissolved gold. The interaction effects of the main factors were found to have a significant effect on the signal intensity, proving that factor values should be jointly optimized instead of one at a time, if maximum ion signal is expected. Optimization of instrumental parameter values was performed for both analyte forms and found to be in a good agreement, indicating a similar behavior of the particles in plasma compared with the dissolved analyte. However, some differences in the behavior of the two analyte forms as regard to sampling depth position was observed. Particle size or the presence of complex sample matrix was not found to influence the optimal instrumental parameter values, however, a significant signal depression for gold was observed (up to 50%) in matrices containing high levels of sodium. Compared to frequently used 'robust conditions', a 70% increase in the ion signal intensity of gold and a 15% decrease in the particle size detection limit was achieved with instrumental parameter optimization. As such, instrumental parameter optimization for sensitive NP analysis can be seen as highly beneficial procedure.

1. Introduction

The remarkable advancements made in the field of nanotechnology have incorporated engineered nanomaterials (ENMs) into our everyday lives. The unique and tunable properties of ENMs have enabled the development of exciting new innovations, which are changing our way to diagnose and treat diseases, produce and store energy and cultivate our lands [1–3]. However, the increasing production of nano-enhanced products has raised concerns about the potential negative effects of these materials on the environment and human health [4–8].

In order to understand the potential impact of nanomaterials on to the environment and human health, it is crucial to characterize these materials carefully. As engineered nanoparticles are produced in various sizes, shapes and with different elemental compositions and surface functionalities, all of which might influence their behavior and effects in the environment [5,6,9,10], characterization of nanoparticles (NPs) can be done in numerous ways. However, as nanomaterial definition is based on size [11], the determination of NP size and number size distribution can be seen as one of the most important parameters to be determined. Several methods are available for NP size characterization, such as microscopic (transmission and scanning electron microscopy (TEM, SEM)), fractionation (hydrodynamic chromatography (HDC) and field-flow fractionation (FFF)) and ensemble methods (dynamic light scattering (DLS) and small-angle X-ray scattering (SAXS)). However, many of the current methods are not well suited for environmental samples [12–15]. The challenge with many currently used methods is that they lack the method sensitivity required for analysis of environmental samples with low NP concentration or may require tedious sample preparation steps, which might lead to sample alteration [13–16].

Single particle inductively-coupled plasma mass spectrometry (spICP-MS) is considered as one of the most promising methods for the determination of NPs, as it is able to overcome many limitations faced with other techniques [17–20]. Compared to other techniques, spICP-MS holds some advantages for NP analysis in environmental samples. Thanks to its sensitivity, spICP-MS enables the measurement of NP size,

* Corresponding author.
E-mail address: virva.v-t.kinnunen@jyu.fi (V. Kinnunen).

https://doi.org/10.1016/j.sab.2021.106104
Received 29 October 2020; Received in revised form 22 January 2021; Accepted 22 January 2021
Available online 30 January 2021

number size distribution, particle number concentration and ionic content at realistic environmental concentrations [17]. In addition, water samples can be analyzed without any sample preparation, which minimizes the risk of altering the state of the NPs. Compared with e.g. microscopic techniques, spICP-MS can provide information of relatively high number of particles in a short period of time (e.g. ≤60s). However, even though particle concentration detection limits in spICP-MS-technique are low (e.g. 100 p/mL) [21], particle size detection limits (LOD_{size}) are often >10 nm for monoisotopic NPs and > 100 nm for oxides [22]. Considering that in the European Commission Recommendation (2011/696/EU) the term 'nanomaterial' is defined as a material containing particles having at least one external dimension in the size range 1–100 nm [11], improving the LOD_{size} can be considered as one of the most important aspects in developing this technique.

The smallest detectable particle size in spICP-MS is determined by the smallest pulse height that can be distinguished from the background and depends mostly on the detection efficiency of the instrument. As such, in terms of lowering the LOD_{size}, improving the ionization conditions and the ion sampling efficiency is crucial. As particles are introduced into the ICP as single droplets, a process of droplet solvation, particle vaporization, atomization and ionization begins [17,23]. As a result, an ion cloud is formed, which diameter will increase as it progresses in the plasma central channel before it is sampled at the sampler orifice. The intensity of the NP signal depends on the relative distance of the ion sampling position (sampler orifice) and the point, where particles start to vaporize. If the signal is measured too early, when vaporization is not complete, the signal will be low. On the other hand, if the signal is measured too late, diffusion losses will be significant, resulting in a decrease in the signal intensity [23–25]. As such, an optimum ion sampling position exists, where ionization has reached its maximum and diffusion losses do not play an effect.

Ionization degree and diffusion losses are affected by particle residence time in the plasma, which is known to be influenced by instrumental parameters, such as nebulizer gas flow, plasma radiofrequency (RF)-power, injector inner diameter (injector i.d.) and sampling depth [23–31]. The optimum value of these parameters depends on a number of factors, including e.g. ionization potential of the element and the boiling point of the corresponding oxide, the size of the introduced droplets and particles and the sample matrix [23,26,29–33]. As such, optimization of instrumental parameters for precise and sensitive NP analysis is crucial. Even though the importance of optimizing instrumental parameters in solution ICP-MS is well-known [32,34–37], the effect of instrumental conditions in spICP-MS are far less studied. In ICP-MS measurements, instrument software's pre-programmed tuning protocols are frequently used for parameter adjustment, which aim to maximize ion signal while minimizing interferences (i.e. 'robust' operation conditions). However, as these protocols are not designed for NP analysis, the adjusted parameters can differ significantly from the optimal values. To the best of our knowledge, only a few articles have focused on studying the effects of instrumental parameters on spICP-MS results. Ho et al. [29] studied the effect of sampling depth values to the intensity of Au and ZrO_2 NPs. Similar optimal sampling depth values were found for dissolved Au and relatively small Au NPs (≤150 nm), however the longer vaporization time of 250 nm Au and 80 nm ZrO_2 NPs resulted in a shift in the optimal sampling depth value as compared to the dissolved analyte. Recently, Kálomista et al. [28] reported that the LOD_{size} for Au and Ag NPs could be significantly improved (25–30%) compared with robust conditions by sampling depth optimization.

As highlighted by Mozhayeva and Engelhard in a recently published review article [38], optimization of instrumental parameters is crucial in order to improve the sensitivity and precision of NP detection. The most critical parameters to optimize are plasma RF-power, sampling depth and nebulizer gas flow, as these are known to affect the ion signal significantly. In addition, the possible effect of the sample matrix and particle size to the optimum conditions should be considered [23,26,29–33]. The traditional optimization method is called as one factor at a time (OFAT) approach, where the optimum value for each factor is determined by varying the value of each factor one at a time [39]. Even though relatively simple to perform, OFAT approach can produce misleading results as it cannot consider any interaction between factors [40]. However, in spICP-MS the effects of instrumental parameters are known to depend on other parameter values (i.e. interaction effects) [25,26], which should be taken into account in optimization studies. This can be achieved by using a design of experiments (DoE) approach, in which the values of factors are varied together allowing one to estimate possible interaction effects between the factors [39,40].

To the best of our knowledge, publications addressing the effects and mutual interactions of plasma RF-power, sampling depth and nebulizer gas flow on spICP-MS analysis do not exist. Hence, the objective of this paper was to optimize these ICP-MS instrumental conditions using a DoE approach. Since gold is one of the most common analytes in spICP-MS, it was selected as the analyte of interest and instrumental parameters for both particulate and dissolved gold were optimized, enabling the comparison between the two. The influence of these parameters on the intensity of particulate and dissolved gold was evaluated in order to assess if dissolved gold could be used in instrument parameter optimization for spICP-MS analysis. The obtained optimum instrumental conditions, as well as the effect on the LOD_{size}, were compared with the robust conditions. Additionally, the possible effect of particle size and sample matrix on optimum instrumental parameter values was evaluated.

2. Experimental

2.1. Materials and methods

2.1.1. Optimization and verification measurements

For optimization measurements, ultra-uniform PEG Carboxyl-stabilized Au NPs with nominal diameter of 50 nm and a solution of dissolved (ionic) gold were used. Au NPs were purchased from PerkinElmer Inc. (Massachusetts, USA) and diluted to a particle concentration of approximately 10^5 particles/g with ultrapure water (resistivity of 18.2 MΩ·cm, PURELAB Ultra, ELGA LabWater, Buckinghamshire, UK). Dissolved gold solution was prepared from a standard stock solution of 100 μg mL^{-1} Au in 2% HCl (Pure Plus, PerkinElmer Inc.) by dilution in ultrapure water to a concentration of 1 μg kg^{-1} and its stability was routinely checked during measurements. Even though dissolved standard solutions are often acidified to improve the analyte stability in the solution [41,42], only ultrapure water was used in all cases for sample dilutions. This allowed the evaluation of the possible differences in the behavior of the two analyte forms, without the risk of incorporating any matrix-induced effects.

For verification of the LOD_{size} under robust and optimal conditions, 20 nm citrate-stabilized (NanoComposix, San Diego, CA, USA) and 30 nm PEG Carboxyl-stabilized (PerkinElmer, Inc.) Au NPs were used. The particle frequency method described by Pace et al. [18] was used to determine the transport efficiency (TE-%) in triplicate using a diluted 50 nm Au NP suspension (PerkinElmer Inc.). All nano-dispersions were diluted to a particle concentration of approximately 10^5 particles/g with ultrapure water. The sample uptake rate was measured in duplicate by weighing the water uptake after 3 min aspiration, and its value was regularly checked during the measurements.

In order to evaluate the possible effects of particle size or sample matrix to the optimal instrumental parameter values, PEG Carboxyl-stabilized Au NPs with nominal diameters of 30, 50 and 100 nm and a solution of dissolved gold (PerkinElmer Inc.) were used. All nano-dispersions were diluted to a particle concentration of approximately 10^5 particles/g and dissolved gold to a concentration 1 μg kg^{-1} with either ultrapure water, 1 mM sodium citrate solution (Sodium Citrate Tribasic Dihydrate from Sigma Aldrich, Darmstad, Germany) or outgoing wastewater. Wastewater was obtained from a municipal wastewater treatment plant located in Central Finland and filtrated with Whatman grade 41 filtration paper before use to remove any solid

material, that might cause blockage of the sample introduction system. Elemental composition of the wastewater used in the experiments was determined with inductively-coupled plasma optical emission spectrometer (PerkinElmer Optima 8300DV ICP-OES) and is presented in Table S1 (Appendix).

All solutions used in the experiments were diluted gravimetrically using new 50 mL polypropylene centrifuge tubes (VWR International) fresh on a daily basis prior to the experiments.

2.1.2. Particle size verification measurements

The certified sizes of the Au NPs used in the experiments were verified in our laboratory (Table S2, Appendix), as at times the standard particle diameters have shown to deviate from the information provided by the manufacturer [12,41,43,44]. Even though microscopic techniques (SEM, TEM) are the common routes used for particle size verification [41,45], the high method detection limit of these techniques made verification of the standard particles with low particle concentration ($\approx 10^7$ particles/mL) impossible. As such, the particle diameters of the PEG Carboxyl-stabilized Au NPs used in the experiments were verified with spICP-MS technique by using citrate-stabilized Au NPs with nominal diameters of 30 and 50 nm (NanoComposix) as a reference. The diameter of these particles was verified with TEM (JEM-1400HC, JEOL, MA, USA) and found to be in good agreement with the values provided by the manufacturer (Table S2, Appendix). The mean particle sizes of the PEG Carboxyl-stabilized Au NPs was found to differ $\leq$3% from the certified values provided by the manufacturer and were use throughout the study.

2.2. Equipment and softwares

A NexION350 D ICP-MS (PerkinElmer Inc., MA, USA) was used in all measurements. Analyses of the NP samples were performed operating the spectrometer in a time-resolved analysis mode using a dwell time of 100 μs, whereas solution mode was used for measurements of the dissolved analyte. General instrumental parameters are shown in Table 1. All data processing was performed using the Syngistix Nano Application Module (v. 2.5) and Microsoft Excel. The isotope ^{197}Au was measured. Minitab 19 software (Minitab, PA, USA) was used for analyzing the experimental data, solving the optimal instrumental parameters and generation of the surface plots.

For measurements performed under 'robust' conditions, a NexION Setup Solution (1 μg L^{-1} Be, Ce, Fe, In, Li, Mg, Pb, and U in 1% HNO_3, Pure Plus, PerkinElmer) was used to adjust the equipment according to instrument software's tuning protocols (maximum sensitivity with CeO^+/Ce^+-level <2.5%) and to check the overall performance. For measurements performed under 'optimal' conditions, the value of nebulizer gas flow was optimized to gain maximum ^{197}Au intensity. Due to the slight day-to-day variations of the instrument condition, the value of nebulizer gas flow was adjusted on a daily basis.

Table 1
Instrumental parameters used in solution ICP-MS and spICP-MS.

	Value[1]	
Parameter	ICP-MS, solution mode	spICP-MS
ICP RF-power (W)	1200–1600 (1000–1600)	1200–1600
Nebulizer gas flow (L min^{-1})	0.90–1.06 (0.80–1.18)	0.90–1.06
Plasma gas flow rate (L min^{-1})	16	16
Auxiliary gas flow rate (L min^{-1})	1.2	1.2
Spray chamber	Baffled Cyclonic, Glass (cooled to 2 °C)	Baffled Cyclonic, Glass (cooled to 2 °C)
Nebulizer	ESI PFA Concentric	ESI PFA Concentric
Injector	1.8 mm i.d. Sapphire	1.8 mm i.d. Sapphire
Sampling depth (mm)	9–12 (9–14)	9–12
Dwell time	50 ms	100 μs
Sampling time (s)		30–60
Transport efficiency (%)		7.48–7.53
Sample uptake rate (g min^{-1})		0.284–0.291

[1] Values shown in brackets used in initial optimization measurements (see Section 3.1).

2.3. Experimental design

The influence of ICP-MS instrumental parameters on the intensity of ^{197}Au was investigated using a DoE approach. Experiments were designed using a general factorial design (GFD), which allows the studied factors to have various, independent levels [39]. Nebulizer gas flow (*A*), plasma RF-power (*B*) and sampling depth (*C*) were chosen as the independent variables and the intensity of gold (^{197}Au) was the response variable (*Y*) measured.

The variables and their levels used for generating the regression models are shown in Table S3 (Appendix). All measurements were performed in a randomized order, except for nebulizer gas flow, to minimize the effect of any uncontrolled factors [46]. Due to a high number of measurements, nebulizer gas flow values were changed from low to high values in all cases in order to save time. Two replicates divided into two blocks were measured in order to increase the precision of the final predictive model. In addition, one experimental point was measured at the beginning and at the end of the 1st and 2nd block, in order to estimate the possible effect of instrumental drift on the response. A total of $2 \times 9 \times 3 \times 3 + 2 = 164$ measurements were performed in this study for both particulate and dissolved gold. The detailed experimental plan and the obtained results are shown in Tables S4 and S5 (Appendix) for particulate and dissolved gold, respectively.

2.4. Statistical analysis

Minitab 19 software was used to analyze the experimental data according to the response surface analysis and to generate surface plots. A second-order polynomial equation was fitted to the experimental data, which is used to express the relationship between the response and the variables. The generalized second-order model has the following form (1):

$$y = \beta_0 + \sum_{i=1}^{k} \beta_i x_i + \sum_{i=1}^{k} \beta_{ii} x_i^2 + \sum \sum_{i<j}^{k} \beta_{ij} x_i x_j + \varepsilon \quad (1)$$

where y is the response (intensity of ^{197}Au), k is the number of variables, x represents the variables, β_0 is the constant term, β_i is the coefficient of the linear parameter, β_{ii} is the coefficient of the quadratic parameter, β_{ij} is the coefficient of the interaction parameters and ε is observed error in the response [39]. Minitab 19 software's response optimization feature was used to solve the optimal instrumental parameters for maximum ^{197}Au response for both particulate and dissolved gold.

3. Results and discussion

3.1. Initial optimization experiments

In the beginning of the study, initial optimization experiments of ICP-MS instrumental conditions were carried out using a solution of dissolved gold (1 μg kg^{-1}). To investigate the influence of ICP-MS instrumental parameters on ^{197}Au intensity, a wide experimental domain was at first monitored (Table 1): plasma RF-power values 1000–1600 W, nebulizer gas flow values 0.80–1.18 L min^{-1} and sampling depth values 9–14 mm, resulting in 400 measurements. During the initial optimization experiments, two main observations were made. First, complex interaction effects between the main factors (nebulizer gas flow, plasma RF-power and sampling depth) were noticed. Secondly, the signal intensity proved to be low at high sampling depth values (>12 mm) and at low plasma RF-value (1000 W). Consequently, a GFD was

chosen to design the experiments using the factor values shown in Table S3 (Appendix). Even though the use of response surface methods with a limited number of measurements are generally more popular approaches in optimization studies, in this case they were found inadequate in describing the changes in the response variable. As in GFD all levels of each factor are combined with all levels of other factors studied, it provides a more detailed description of the change in the response variable in accordance with the variables studied.

3.2. Fitting a second-order polynomial equation and model adequacy checking

To relate the measured intensity to the variables, a second-order polynomial model was fitted to the data according to Eq. (1). In order to improve the model for operating conditions, the statistically insignificant terms were automatically removed using a backward elimination process available in Minitab 19 software. This procedure automatically excludes certain terms from the regression model, which are not found to have statistically significant impact on the response at the chosen 95% confidence level (i.e., variables with P-values <0.05). For both forms of the analyte, the interaction effect of plasma power (*B*) and sampling depth (*C*) was found statistically insignificant at the 95% confidence level. In addition, no statistically significant difference was found between the two blocks, indicating that the results obtained for the two replicates were in good agreement. As such, these variables were removed from the final regression models.

The significance of the final fitted regression models, main factors and their interactions was evaluated on the basis of analysis of variance (ANOVA), which are presented in Tables S6 and S7 (Appendix) for particulate and dissolved gold, respectively. The statistical significance of the different terms was evaluated using the corresponding P-values, with 95% confidence level as the chosen significance level (P = 0.05). The resulting models have large F-values (287.68 for particulate and 335.05 for dissolved gold) and P-values < 0.05, indicating that the models are able to explain the observed variation in the response and can be used to optimize the conditions. In the final models, the main and quadratic effects of the studied variables (nebulizer gas flow (*A*), plasma RF-power (*B*) and sampling depth (*C*) and A^2, B^2 and C^2) were found to have significant effects on the response (intensity of ^{197}Au) for both particulate and dissolved gold. Of the two-level interaction terms, the interaction effect of nebulizer gas flow and plasma RF-power (*A*B*) and nebulizer gas flow and sampling depth (*A*C*) were found statistically significant at the 95% confidence level.

For testing the goodness of fit of the regression equations, the R-values were evaluated. For both of the models, R^2-and adjusted R^2-values are >93% indicating a good agreement between experimental and predicted values. The models' ability to predict the responses for the new observations accurately can be estimated on the basis of R^2(pred.)-value, which in this case were high for both models; >92%. The P-value for the lack-of-fit is >0.05, indicating that the proposed models are able to specify the relationship between the response and the variables correctly. Model assumption checks and the main effects plots for both models are presented in Figs. S1–S4 (Appendix).

The final predictive equations obtained for the particulate and dissolved gold in uncoded units were obtained as follows:

Particulate gold:

$$Y(counts) = -3217 + 9411A - 1.899B - 13.2C - 7604A^2 - 0.000192B^2 - 10.071C^2 + 2.5117A*B + 198.3A*C \quad (2)$$

Dissolved gold:

where Y is the intensity of ^{197}Au (in counts), A is the nebulizer gas flow (L min^{-1}), B is the plasma RF-power (W) and C is the sampling depth (mm).

3.3. Effect of instrumental parameters on Au intensity

The obtained second-order polynomial equations presented in the previous section (Eqs. (2) and (3)) were used for generating response surface plots (Fig. 1A–F), which can be used to investigate the effect of instrumental parameters on the response. In each surface plot, the value of one variable is kept fixed at a constant value, allowing one to consider the effects of the other two variables. In order to evaluate the behavior of the two analyte forms under optimal instrumental conditions, in each surface plot the value of the 3rd variable was kept fixed at its predicted optimal value (as determined in Section 3.4).

In Fig. 1A and B the effect of nebulizer gas flow and plasma RF-power on the measured intensity of particulate and dissolved gold is presented. In order to evaluate the behavior of the two analyte forms under the optimal instrumental conditions (as determined in Section 3.4), the value of sampling depth is kept fixed at its predicted optimal value (11.0/10.0 mm for particulate and dissolved gold, respectively). High similarity in the surface plots can be seen, indicating a similar behavior of both forms of the analyte as the factor values are changed. Clearly, the interaction effect of these two variables has a major effect on the intensity value of gold and the overall effect of changing one factor value is highly dependent on the value of the other variable. As expected, the measured intensity generally increases when using higher power values due to higher ionization efficiency of the analyte [27,34–36,47]. However, due to a significant interaction effect of the two variables, the optimal value of nebulizer gas flow depends on the applied power (and vice versa). As plasma power is increased, the optimal flow shifts to larger values due to changes in plasma characteristics [36,47]. The value of nebulizer gas flow is known to influence analyte transport through plasma and the axial plasma temperature, thus affecting the analyte residence time in the plasma. As the value of nebulizer gas flow is increased, the maximum temperature of the plasma central channel decreases and the atomization position will shift downstream the plasma closer to the sampler cone orifice [26,36,47,48]. If a low nebulizer gas flow value is used, increasing the plasma RF-power will cause the sample to ionize immediately after entering the plasma, i.e., at a position distant from the sampler orifice resulting to diffusion losses and a decrease in signal intensity [23,24,26,30,47]. For both forms of the analyte, at the given sampling depth value, the maximum intensity values can be found at plasma RF-power 1600 W and nebulizer gas flow value of 1.01–1.03 L min^{-1}.

The interaction effect of nebulizer gas flow and sampling depth can be investigated from Fig. 1C and D for particulate and dissolved gold, respectively. In both cases, plasma RF-power is held constant at its predicted optimal value of 1600 W. For both forms of the analyte, a general increase in the intensity is observed as larger values of nebulizer gas flow are used, with optimal area found at flow rates >1 L min. Even though decreasing the sampling depth position generally results in an increase in the intensity at low nebulizer gas flow values (≈<1 L min^{-1}), at higher gas flow rates the optimal value of sampling depth is shifted to larger values. This is because as the value of nebulizer gas flow is increased, the ionization degree of the analyte decreases as the interaction time of the analyte with the hot plasma decreases [23,26,36,47]. As a consequence, in order to compensate the temperature drop caused by a larger volume of gas injected, longer residence time (i.e. sampling depth) is needed for complete vaporization and ionization [23,25,26,30]. For both forms of the analyte, highest intensity values are found at nebulizer gas flow values >1 L min^{-1} and at sampling depth

$$Y(counts) = 1\,745\,603 + 5\,070\,025A - 998.6B + 12\,810C - 4\,090\,912A^2 - 0.1255B^2 - 5422C^2 + 1417.0A*B + 94\,268A*C \quad (3)$$

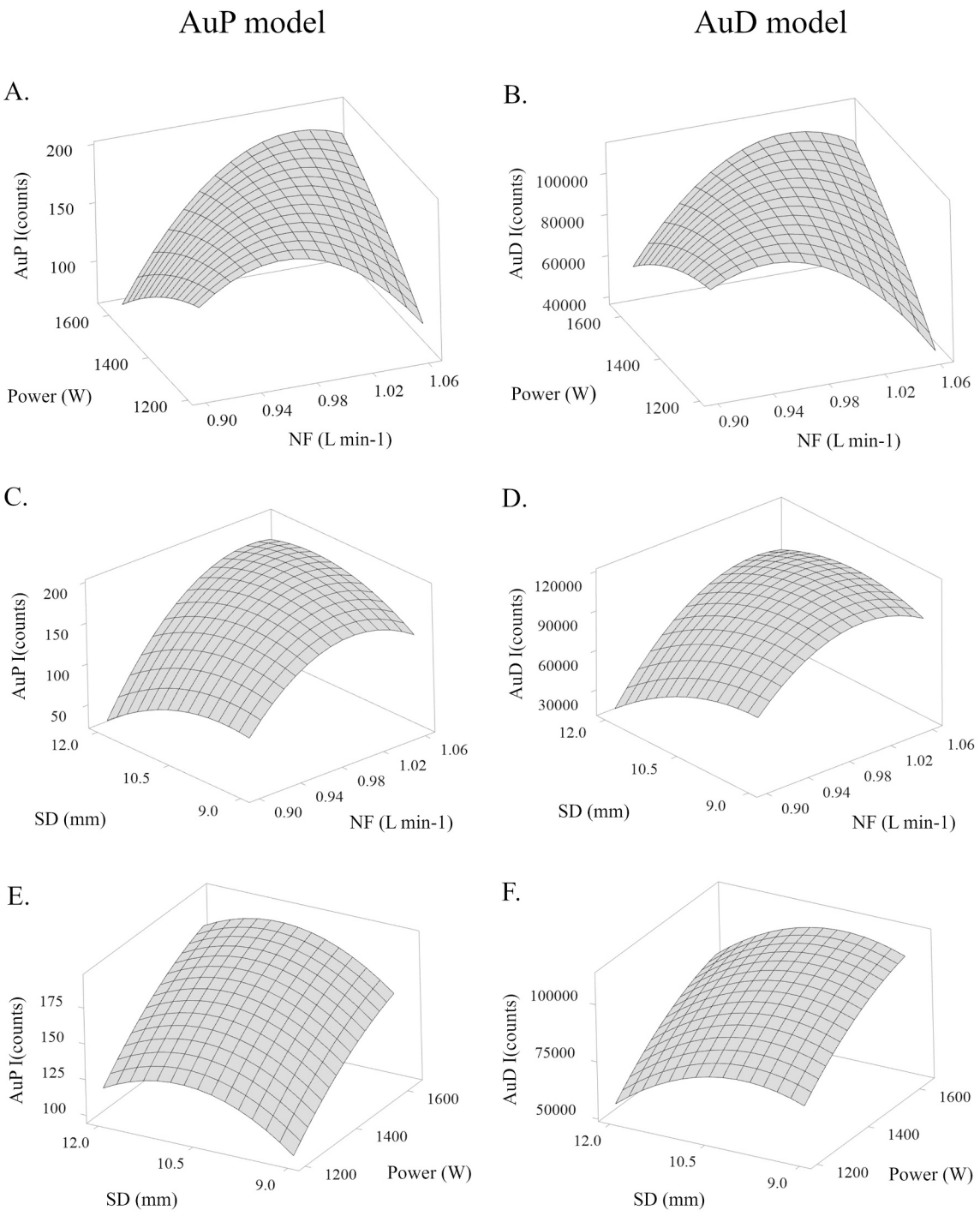

Fig. 1. Response surface plots showing the individual and interaction effects of A, B) Nebulizer gas flow (NF, L min^{-1}) and RF-power (power, W); C, D) Nebulizer gas flow (L min^{-1}) and sampling depth (SD, mm) and E, F) RF-power (W) and sampling depth (mm) on the measured intensity of gold. In each surface plot, one variable is kept constant as follows (for particulate/dissolved gold): Nebulizer gas flow 1.03/1.01 L min^{-1}, RF-power 1600 W and sampling depth 11.0/10.0 mm. Response surface plots for particulate gold (AuP) are shown on the left, and for dissolved gold (AuD) on the right side of the figure. (For interpretation of the references to colour in this figure legend, the reader is referred to the web version of this article.)

values 10–11 mm.

When comparing the response surface plots drawn for particulate and dissolved gold (Fig. 1C and D), high similarity in the graphs can be seen. However, some minor differences as regard to the effect of the sampling depth position can be observed. For dissolved gold, at the vicinity of maximum intensity area (Fig. 1D, at nebulizer gas flow rates $\geq$1 L min^{-1}), only minor differences in the intensity are observed at sampling depth range 9–11 mm. However, a decrease in intensity is observed for particulate gold as the value of sampling depth is decreased <10 mm. It seems that the intensity of particulate gold is somewhat more dependent on the effect of these two variables. As discussed before, increasing the nebulizer gas flow value has the effect of decreasing plasma temperature and increasing analyte velocity through plasma, thus shifting the point of atomization closer to sampler cone orifice [26,36,48]. As particles are expected to require longer time for complete vaporization and atomization [23,26,33,47,49], larger sampling depth

values might be required for efficient ionization. In addition, as sampling depth is increased, the temperature of the plasma has shown to increase [29,31], leading to an increase in the ionization degree.

The difference in the behavior of the two analyte forms as regard to the sampling depth position can be more clearly seen in Fig. 1E and F, where the interaction effect of plasma RF-power and sampling depth is presented. The value of nebulizer gas flow is kept fixed at its predicted optimum value (at 1.03/1.01 L min^{-1} for particulate and dissolved gold, respectively). For both forms of the analyte, increasing plasma RF-power results to a significant increase in the intensity value independent on the applied sampling depth position. However, the value of sampling depth position has clearly different effect on the intensity of the two analyte forms. Whereas for dissolved gold decreasing the sampling depth value generally results in an increase in the intensity value, for particulate gold the intensity is observed to decrease. In contrast to dissolved gold, the highest intensity values for particulate gold are found at slightly larger sampling depth values (11 mm as contrast to 10 mm). This might be because of the longer residence time needed for complete vaporization and atomization of the particles, as discussed previously. However, as can be seen in Fig. 1F, only minor differences are observed in the intensity of dissolved gold at the sampling depth range 9–11 mm.

Based on the obtained results, the interaction effects of the main variables clearly have a significant effect on the intensity of gold for particulate and dissolved gold. As the overall effect of adjusting instrumental parameter values is dependent on other parameter values, careful optimization of factors is crucial if maximum ion signal is expected. For both forms of the analyte, the highest intensity values can be achieved by using high plasma RF-power (1600 W) and sampling depth value of 10–11 mm. For a given plasma RF-power and sampling depth value, a narrow area of optimal nebulizer gas flow value is found, as already noticed for solution ICP-MS [34,35]. Deviation from the optimal values could result in a loss of intensity and thus increase in the LOD_{size}.

When comparing the response surfaces generated for particulate and dissolved gold, high similarity between the graphs can be seen. However, regarding the sampling depth position, some minor differences in the behavior of particulate and dissolved gold was observed. As the vaporization and ionization of the particles require somewhat longer times as compared to the dissolved analyte [23,26,33,47,49], the optimal sampling depth value for Au NPs was found at slightly higher values (11 mm as compared to 10 mm). However, as seen in Fig. 1D and F, adjusting the sampling depth position at the range of 9–11 mm was not found to impact the intensity of dissolved gold to a large extend. As such, the predicted optimal instrumental parameters can be expected to be similar for Au NPs and dissolved gold with some minor differences in the optimal sampling depth positions.

3.4. Optimization of instrumental parameters

The predicted optimal instrumental parameters for the measurement of particulate and dissolved gold were solved with Minitab 19 software's response optimizer feature, which automatically solves the optimal set of parameter values producing the maximum responses of Eqs. (2) and (3) (see Section 3.2). The predicted optimal instrumental parameter values were as follows (for particulate/dissolved gold): nebulizer gas flow value 1.03/1.01 L min^{-1}, plasma RF-power 1600 W and sampling depth 11.0/10.0 mm. In order to verify the optimal instrumental conditions, the intensities of both particulate and dissolved gold were measured under the predicted optimal conditions and the obtained experimental intensities were compared with the predicted values (Table S8, Appendix). Even though the optimization and verification measurements were performed on different days and as such were susceptible to the day-to-day variation in the general intensity level, the obtained values were observed to differ <9% from the predicted values. In addition, as the measured intensities fell under the 95% prediction interval (represents the range of values where a single new observation is likely to fall with 95% confidence), the acquired regression models can be concluded to be reasonably accurate for predicting the ^{197}Au intensity with optimized instrumental parameters for both forms of the analyte.

As regard to the predicted optimal values of sampling depth and nebulizer gas flow rate, slight differences are found for particulate and dissolved gold. However, as discussed before and seen on Fig. 1D and F, at plasma power 1600 W, the predicted differences in the intensity of dissolved gold at the sampling depth range of 9–11 mm are expected to be small and thus could be attributed to the uncertainty of the regression model. As such, an additional experiment was performed in order to verify the optimal values for sampling depth and nebulizer gas flow and to evaluate the effect of the different experimental conditions. The intensity of particulate and dissolved gold was thus measured at sampling depth positions 9–12 mm (with an increment of 1 mm) with plasma power set to its optimal value of 1600 W. As already discussed in Section 3.3 and seen in Fig. 1 C and D, the optimal value of nebulizer gas flow is highly dependent on the applied sampling depth position. As such, in order to find the maximum intensity at different conditions, the value of nebulizer gas flow was separately optimized for every sampling depth position. Measurements were performed in triplicate in a randomized order to minimize the effect of any uncontrollable factors on the results. The detailed experimental plan and the obtained results are presented in Tables S9 and S10 (Appendix), respectively, and displayed in Fig. 2.

As can be seen in Fig. 2, for both forms of the analyte the highest intensity values are obtained at sampling depth position of 11.0 mm. As the sampling depth position is altered from the optimum value, the intensity value is observed to decrease up to 10%. However, especially for dissolved gold, the differences in the intensities between sampling depth positions 10 and 11 mm are found to be extremely small (<5%), which could explain the observed differences in the predicted optimal instrumental parameter values for the two analyte forms. For particulate gold however, as already seen in Fig. 1C, the optimal sampling depth value range is more narrow and decreasing the SD value <11 mm results up to a 10% decrease in the intensity.

When comparing to robust conditions (i.e. conditions where nebulizer gas flow was adjusted to gain maximum ^{115}In sensitivity and $CeO^+/$

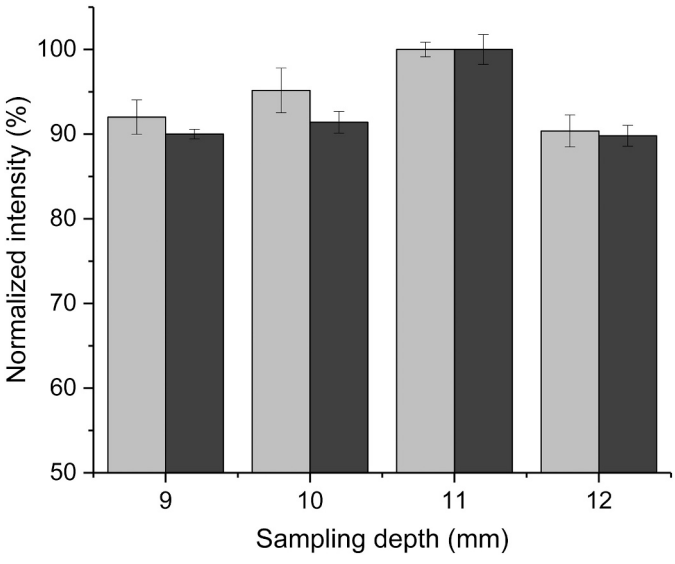

Fig. 2. The obtained maximum intensity of particulate (dark grey bars) and dissolved (light grey bars) gold at different sampling depth positions, presented as mean of three replicate measurements ± relative standard deviation (σ_r). At each sampling depth position, the measured intensity is presented as normalized intensity (%) against the obtained highest intensity value over the entire region, which for both forms of the analyte is obtained at sampling depth value of 11.0 mm. (For interpretation of the references to colour in this figure legend, the reader is referred to the web version of this article.)

Ce^+ <2.5%), the optimization of instrumental parameters resulted in an increase in the nebulizer gas flow value. One should note that as the instrumental parameter values are changed, interferences arising from oxides and double-charged ions should be considered. For some analytes, such as Ti and Fe, these plasma- and/or sample matrix-based interferences can have a severe impact on the accuracy of the results, and the use of collision or reaction gases (e.g. He, NH_3) for interference elimination might be needed [50,51]. However, in the case of analysis of Au NPs from environmental samples, the influence of these interferences (mainly $^{181}Ta^{16}O^+$) can be seen as insignificant. Decreasing sampling depth value from the robust setting (11 mm) was not found to improve the ion signal. This is somewhat in contrast to results obtained by Kálomista et al. [28], who found that NP signal can be significantly improved by sampling depth optimization (from 10 mm to 4 mm). The differences in the findings could arise from differences in instrumental configurations (e.g. sample introduction system) or, more likely, from the chosen optimization method. When optimization of sampling depth is performed by keeping all other instrumental parameter values fixed at a constant value, the interaction effects of the factors cannot be considered. Using this approach, the intensity of both forms of the analyte was found to increase as the value of sampling depth was decreased [28]. This is consistent with our findings at low nebulizer gas flow values (<1 L min^{-1}, see Fig. 1 C and D). However, due to interaction effects of the factors observed in this study, the true maximum intensity values were found at higher nebulizer gas flow (>1 L min^{-1}) and sampling depth values.

3.5. Effect of optimization on instrument sensitivity and on size detection limits

As discussed in Section 1, LOD_{size} (calculated as the particle size equivalent of three times the standard deviation of the blank of the particle calibration plot [17,18,52]) could be significantly improved by careful optimization of instrumental parameters. In order to evaluate the effect of instrumental parameter optimization to instrument sensitivity and LOD_{size}, particle calibration in the range 0–100 nm under optimized and robust conditions was performed and presented in Fig. S5 (Appendix). Under the optimized instrumental conditions, a significant (70%) increase in the instrument sensitivity was observed as compared to robust conditions, which translates in to a 16% decrease in the theoretical size detection limit, $LOD_{size(Theor.)}$ (from 10.4 nm to 8.7 nm). It should however be noted, that instrument software's Nano Application module was used to automatically calculate the $LOD_{size(Theor.)}$, where the smallest observed pulse intensity originating from particles is converted to particle mass and diameter using a calibration curve. The threshold limit used to discriminate the particle signals from the background signal is determined using an iterative 'mean+3σ' computation [53]. However, as the theoretical $LOD_{size(Theor.)}$ is calculated based on the measured intensities of the calibration blank, highly optimistic values are often obtained and at times some manual adjustment is required. During the measurements under this study, intensity values ≤2 counts with mean of ≈ 0 counts were obtained for the calibration blanks, resulting to a particle threshold of just 1 count. As such, particle intensity threshold limit was manually increased to 3 counts, converting to adjusted $LOD_{size(Adj.)}$ values of 13 and 15 nm under optimal and robust conditions, respectively.

In order to verify the estimated LOD_{size} values obtained under the different instrumental conditions, Au NPs with nominal diameter of 20 nm was measured in triplicate under optimal and robust conditions. The in-lab verified diameter of this particle is 18.9±1.9 (Table S2, Appendix), i.e., practically at the LOD_{size}. The obtained particle size frequency distribution for one of the replicates under optimal and robust conditions is presented in Fig. 3. For comparison purposes, measurements were performed also for 30 nm PEG-Carboxyl-stabilized Au NP. The obtained experimental results for the NPs under different conditions were compared as regard to particle concentration yield and particle size

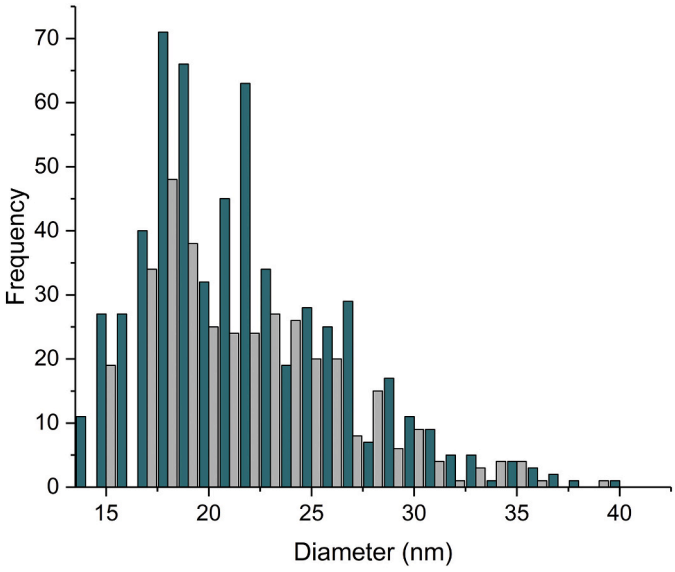

Fig. 3. Obtained particle size frequency distribution graph for 20 nm Au NP under optimal (green bars) and robust (grey bars) conditions. Instrumental parameters were set as follows (for optimal/robust conditions): Plasma RF-power 1600 W/1600 W; nebulizer gas flow 1.02/0.93 L min^{-1} and plasma sampling depth 11/11 mm. (For interpretation of the references to colour in this figure legend, the reader is referred to the web version of this article.)

and presented in Table S11 (Appendix). Under optimal instrumental conditions, the determined particle diameter was closer to the expected value and a 20% increase in the particle concentration yield was observed as compared to robust conditions. The higher particle concentration yield achieved under the optimal instrumental conditions results from the significantly increased sensitivity, allowing more particles to be detected over the background signal. However, under both conditions particle concentration yields <30% were obtained. When comparing the obtained results for the 30 nm Au NP under optimal and robust conditions, no significant differences are observed and particle concentration yields of 101% were achieved. This indicates that the experimental results obtained for particles <30 nm should be interpreted with caution, as low particle concentration recoveries might occur.

Clearly, the determination of small particles near the LOD_{size} is challenging and estimation of the particle concentration near this value should be done with caution. Even though optimization of instrumental parameters resulted in a significant increase in instrument sensitivity and thus in decrease in the LOD_{size}, low particle concentration yields were achieved for the 20 nm Au NPs under both conditions. The determination of particle concentration of particles with diameters close to the LOD_{size} is problematic, as the LOD_{size} cannot be interpreted as straightforward as in solution mode ICP-MS (i.e., concentrations >LOD visible and <LOD unvisible). The same observation was made recently by Mastek et al. [54], who reported particle concentration yields as low as 5% for particles with diameters close to the LOD_{size}. The reason why small particles near the LOD_{size} behave in such unexpected manner, remained unclear. According to some authors [41,52,54,55], particle size or surface could affect the transport efficiency value, which could in part explain the observed results. However, in this paper, these factors were not studied further. More research concerning the detection of small particles and the factors affecting the accuracy of the results is clearly needed.

3.6. Effect of particle size and matrix

As already discussed in Section 1, the sample matrix and sample mass could lead to differences in the optimal instrumental conditions. This is

because these are shown to affect the plasma characteristics and the required particle residence time in the plasma [33,56,57]. As larger particles require more time for complete atomization, under certain instrumental conditions incomplete ionization could occur, especially if low sampling depth values are used. This could cause the measured intensity to be lower than expected and thus lead to non-linear calibration curves [23,25,30,31]. In addition, the sample matrix could affect the position, where analyte atomization begins, by cooling the plasma locally or by affecting the introduced droplet size. As the time needed for complete desolvation of larger droplets is found to be longer, they penetrate deeper into ICP and thus the point of the analyte atomization is shifted closer to the sampler orifice [26,56].

As such, the sample matrix and particle size could affect the optimal instrumental parameter values and the linearity of the particle calibration curve. To investigate the possible effect of particle size and sample matrix to the optimal sampling depth values, the intensity of particulate (30 nm and 100 nm) and dissolved gold was measured in several matrices at different sampling depth positions: ultrapure water, wastewater and 1 mM trisodium citrate solution (TSC). The elemental composition of the wastewater matrix used in the experiments is presented in Table S1 (Appendix). Measurements were performed using a nebulizer gas flow value optimized for sampling depth 11.0 mm at RF-power 1600 W. The results are presented in Fig. 4 A–C and in supplementary material (Table S12 and Fig. S6, Appendix).

As the results show, the signal behavior of particulate and dissolved gold is highly similar, as shown already in Section 3.3 and noticed by other research groups as well [28–30], indicating that optimal instrumental conditions are in fact the same for both forms of the analyte. Matrix is not found to affect the behavior of the two analyte forms in different extents, and in all cases the largest intensity values are found at sampling depth value 11.0 mm for both particulate and dissolved gold. In addition, the behavior of the different sized particles (30 and 100 nm) is highly similar and no differences are observed in the optimal sampling depth position. This indicates that vaporization even of the larger particles (100 nm) under the experimental conditions had reached its maximum in all of the studied matrices. Interestingly, even though no differences were observed in the behavior of different forms of the analyte as regard to the sampling depth position, some differences were found between the matrices. Whereas in ultrapure water and in TSC solution the intensity of both forms of the analyte is observed to decrease up to 50% as sampling depth is increased from 11 mm to 14 mm, only 40% decrease is observed in the wastewater matrix. This might be because the ionization of the various elements present in wastewater (Table S1, Appendix) consume plasma energy, shifting the position of atomization closer to the sampler cone orifice and thus minimizing the diffusion losses [26,56].

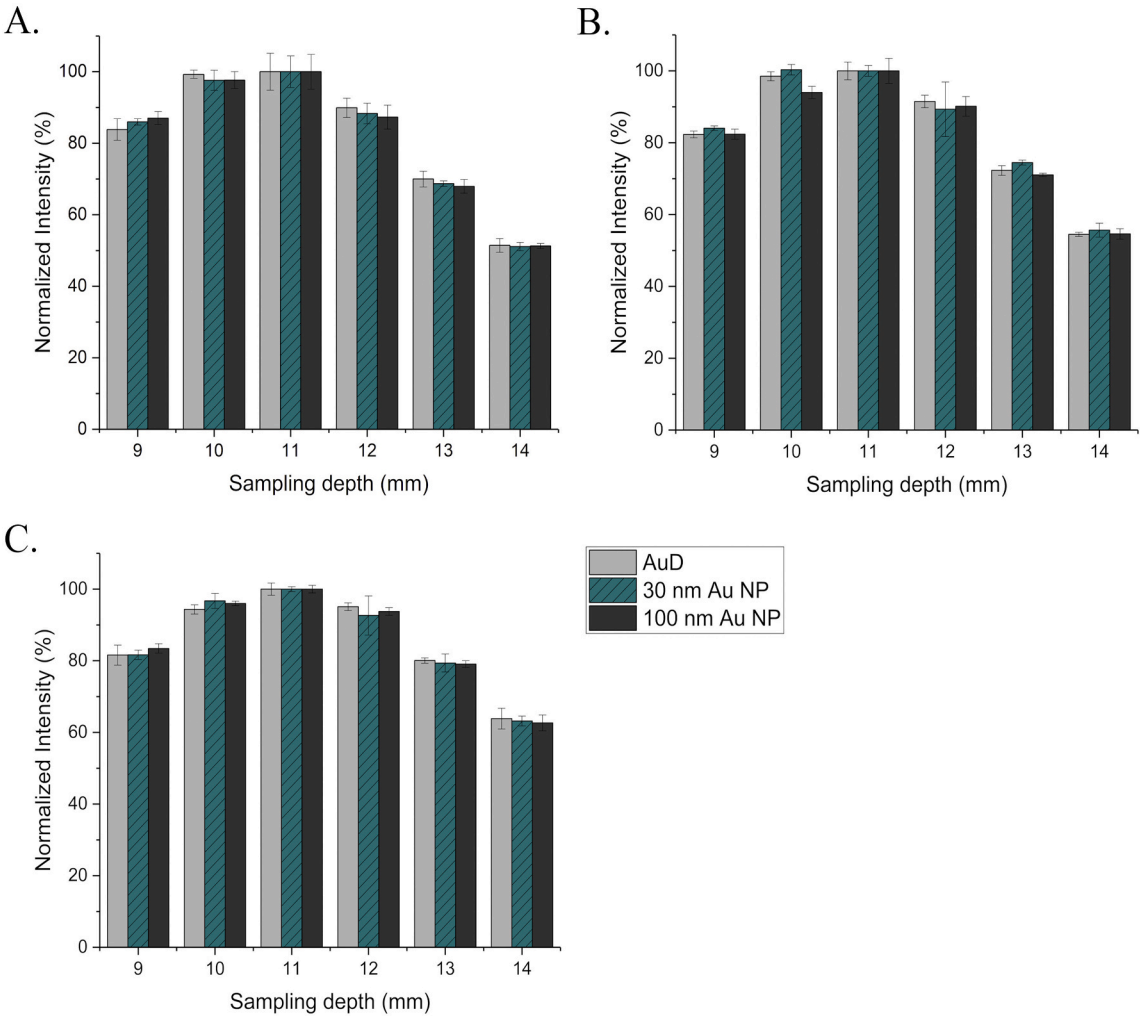

Fig. 4. The intensity of particulate (30 and 100 nm Au NP) and dissolved gold (AuD) in different matrices as a function of sampling depth, presented as mean of three replicate measurements ± relative standard deviation (σ_r). Results are normalized to the highest intensity value (100%). A) Ultrapure water, B) 1 mM Trisodium citrate solution and C) Wastewater. Light grey: Dissolved gold (AuD), green with diagonal lines: 30 nm Au NP and dark grey: 100 nm Au NP. Measuring parameters were set as follows (for particulate/dissolved gold): Plasma RF-power 1600 W/1600 W and nebulizer gas flow 1.02 L min^{-1}/1.01 L min^{-1}. (For interpretation of the references to colour in this figure legend, the reader is referred to the web version of this article.)

When comparing the obtained intensity values (Table S12 and Fig. S6, Appendix) in the different matrices, a significant signal depression in the wastewater and TSC matrices as compared to ultrapure water is observed. For both forms of the analyte, up to a 50% decrease in the intensities is observed in the wastewater matrix. In the TSC matrix, intensities were found to decrease up to 25% as compared to ultrapure water, however, only for particulate gold. The observed signal depression is most likely caused by the high level of sodium present in these matrices (70 mg L^{-1} in TSC solution and 180 mg L^{-1} in wastewater). Sodium is a known source of non-spectral interferences in spICP-MS-measurements, which' depressive effect is shown to increase with increasing concentration [58,59], consistent with our findings. As no significant signal depression was found for dissolved gold in TSC solution, it can be assumed, that the intensity of particulate gold is more affected by the matrix elements. It should be noted that differences in the sensitivities between particulate and dissolved analyte could lead to biased results, if dissolved calibration curve is used to determine particle size or transport efficiency. As such, the effect of sample matrix should be investigated in the early stages of method development process. Sample dilution or matrix matching between the sample and standard solutions can be used as a means to avoid systematic errors. However, is some cases these procedures cannot be applied or are found insufficient, as would be the case if the two analyte forms are affected by the matrix elements in different extends. Clearly, the matrix interferences are one of the remaining challenges in the spICP-MS-technique requiring more research in the future.

As discussed before, under certain instrumental conditions incomplete ionization or diffusion losses of the different-sized particles could occur. This could lead to non-linear particle calibration curves, as in spICP-MS particle calibration is based on a fact that measured intensity is directly proportional to the mass of an element [17]. As such, the effect of particle size on the linearity of the calibration curve under the optimized instrumental conditions in the range 0–100 nm was studied and presented in Fig. S5 (Appendix). As calibration was found to be linear over the studied range, it can be concluded, that for $\leq$100 nm particles vaporization has reached its maximum at the instrumental conditions used and no clear indication of diffusion losses of the smaller particles can be seen. However, larger particles ($\geq$100 nm) might not vaporize completely at the instrumental conditions used, which should be considered if large (>100 nm) particles are analyzed.

4. Conclusions

In this paper, the optimization of spICP-MS instrumental parameters was performed using a DoE approach for particulate and dissolved gold, enabling the evaluation of the behavior of the two analyte forms as the factor values are changed. The variables studied were nebulizer gas flow, plasma RF-power and sampling depth, as these are known to affect the ion signal most. Results show that significant interaction effects between the main factors exists and clearly have a major effect on the intensity of gold for both forms of the analyte. As the overall effect of a parameter is highly dependent on other parameter values, changing the value of one parameter can result in a loss of intensity, if the other variables are not re-optimized. As such, traditional OFAT approaches are not suitable for spICP-MS optimization, as they cannot estimate the interaction of the factors and thus can produce misleading results.

In order to assess the possible differences in the behavior of the two analyte forms, the effect of instrument parameter values on the intensity of particulate and dissolved gold was evaluated. High similarity in the behavior of both forms of analyte in accordance with the variables was noticed, indicating that dissolved analyte can in fact be used in method optimization. Compared with nano-dispersions, the possibility to use dissolved analyte offers some benefits, such as better stability of the standard solutions and faster measurements. However, as regard to the effect of sampling depth position, some minor differences in the behavior of the analyte forms was observed. For dissolved gold at the vicinity of optimal conditions (plasma RF-power 1600 W and nebulizer gas flow values >1 L min^{-1}) adjusting the value of sampling depth had only minor effects on the intensity. However, as a result of longer residence time needed for efficient atomization, the intensity of particulate gold was observed to decrease at lower sampling depth positions.

The optimal instrumental parameters were solved and verified for both forms of the analyte and were as follows: Plasma RF-power 1600 W, sampling depth 11.0 mm and nebulizer gas flow 1.01–1.03 L min^{-1}. Due to the slight day-to-day variation of the instrument condition (e.g. the cleanliness of the sample introduction system), the optimal nebulizer gas flow value should however be routinely checked and re-optimized if necessary. One should note that optimal instrumental parameter values are analyte and instrument-specific, and should be optimized in the early stages of a method development process. In addition, the possible interferences caused by oxide- and double charged ions should be considered, especially in the case of more challenging analytes such as Fe and Ti.

The influence of instrument parameter optimization on the LOD_{size} was evaluated. Compared with robust conditions often used, instrument sensitivity was improved by 70% and LOD_{size} by approximately 15% (from 15 nm to 13 nm). Even though more particles were detected under optimal conditions as a result of significantly increased sensitivity, particle concentration yields <30% were achieved for particles with diameter close to the LOD_{size}. Clearly, the determination of small particles near the LOD_{size} value is challenging and estimation of particle concentration needs to be made with caution. The same observation has been made by other authors as well, indicating that more research on determination of small particles near LOD_{size} is urgently needed.

Finally, the influence of solution matrix and particle size to the optimal instrumental parameter values was studied. Neither particle size nor sample matrix was observed to influence the optimal instrumental conditions, indicating that the behavior of both forms of analyte is highly similar and even the larger particles ionize completely under the instrumental conditions used. However, due to the high level of sodium (180 mg L^{-1}) present in the wastewater matrix, a significant signal depression (up to 50%) for both particulate and dissolved gold was observed in the wastewater matrix as compared to ultrapure water. Similarly, up to a 25% decrease in the intensity was observed in the TSC solution, however, only for particulate gold. It seems that particulate gold is more susceptible to matrix effects, as the intensity of dissolved gold was not affected in the TSC solution containing 70 mg L^{-1} of sodium. As sodium is a common element present in both biological and environmental samples, its effect on analyte sensitivity should be investigated and care should be taken to match the sample and standard solution matrices to avoid systematic errors.

Declaration of Competing Interest

The authors declare that they have no known competing financial interests or personal relationships that could have appeared to influence the work reported in this paper.

Acknowledgements

This work was supported by the University of Jyväskylä (Finland), Department of Chemistry. Sini Reuna and Joona Rajahalme are greatly appreciated for their helpful comments regarding the manuscript and discussions regarding the experimental results.

Appendix A. Supplementary data

Supplementary data to this article can be found online at https://doi.org/10.1016/j.sab.2021.106104.

References

[1] M.C. Roco, C.A. Mirkin, M.C. Hersam, Nanotechnology research directions for societal needs in 2020: summary of international study, J. Nanopart. Res. 13 (2011) 897–919, https://doi.org/10.1007/s11051-011-0275-5.

[2] European Chemicals Agency (ECHA), European Union Observatory for Nanomaterials, (n.d.). https://euon.echa.europa.eu/ (accessed February 7, 2020).

[3] Project on Emerging Nanotechnologies. Consumer Products Inventory. (n.d.) http://www.nanotechproject.org/cpi/, 2013s, (accessed April 7, 2020).

[4] E.A.J. Bleeker, S. Evertz, R.E. Geertsma, W.J.G. Peijnenburg, J. Westra, S.W. P. Wijnhoven, Assessing Health & Environmental Risks of Nanoparticles, Report No. 2014-0157, National Institute for Public Health and the Environment, Bilthoven, The Netherlands, 2015.

[5] J.R. Lead, G.E. Batley, P.J.J. Alvarez, M.N. Croteau, R.D. Handy, M.J. McLaughlin, J.D. Judy, K. Schirmer, Nanomaterials in the environment: behavior, fate, bioavailability, and effects—an updated review, Environ. Toxicol. Chem. 37 (2018) 2029–2063, https://doi.org/10.1002/etc.4147.

[6] E. Kabir, V. Kumar, K.H. Kim, A.C.K. Yip, J.R. Sohn, Environmental impacts of nanomaterials, J. Environ. Manag. 225 (2018) 261–271, https://doi.org/10.1016/j.jenvman.2018.07.087.

[7] K. Savolainen, H. Alenius, H. Norppa, L. Pylkkänen, T. Tuomi, G. Kasper, Risk assessment of engineered nanomaterials and nanotechnologies-a review, Toxicology 269 (2010) 92–104, https://doi.org/10.1016/j.tox.2010.01.013.

[8] K.L. Garner, S. Suh, A.A. Keller, Assessing the risk of engineered nanomaterials in the environment: development and application of the nanoFate model, Environ. Sci. Technol. 51 (2017) 5541–5551, https://doi.org/10.1021/acs.est.6b05279.

[9] A. Albanese, P.S. Tang, W.C.W. Chan, The effect of nanoparticle size, shape, and surface chemistry on biological systems, Annu. Rev. Biomed. Eng. 14 (2012) 1–16, https://doi.org/10.1146/annurev-bioeng-071811-150124.

[10] A.L. Dale, E.A. Casman, G.V. Lowry, J.R. Lead, E. Viparelli, M. Baalousha, Modeling nanomaterial environmental fate in aquatic systems, Environ. Sci. Technol. 49 (2015) 2587–2593, https://doi.org/10.1021/es505076w.

[11] The European Commission, Off. J. Eur. Union 696, 2011, pp. 38–40.

[12] A.R. Montoro Bustos, K.P. Purushotham, A. Possolo, N. Farkas, A.E. Vladár, K. E. Murphy, M.R. Winchester, Validation of single particle ICP-MS for routine measurements of nanoparticle size and number size distribution, Anal. Chem. 90 (2018) 14376–14386, https://doi.org/10.1021/acs.analchem.8b03871.

[13] Y.-J. Chang, Y.-H. Shih, C.-H. Su, H.-C. Ho, Comparison of three analytical methods to measure the size of silver nanoparticles in real environmental water and wastewater samples, J. Hazard. Mater. 322 (2017) 95–104, https://doi.org/10.1016/j.jhazmat.2016.03.030.

[14] K. Tiede, M. Hassellöv, E. Breitbarth, Q. Chaudhry, A.B.A. Boxall, Considerations for environmental fate and ecotoxicity testing to support environmental risk assessments for engineered nanoparticles, J. Chromatogr. A 1216 (2009) 503–509, https://doi.org/10.1016/j.chroma.2008.09.008.

[15] F. Laborda, E. Bolea, G. Cepriá, M.T. Gómez, M.S. Jiménez, J. Pérez-Arantegui, J. R. Castillo, Detection, characterization and quantification of inorganic engineered nanomaterials: a review of techniques and methodological approaches for the analysis of complex samples, Anal. Chim. Acta 904 (2016) 10–32, https://doi.org/10.1016/j.aca.2015.11.008.

[16] M. Hassellöv, J.W. Readman, J.F. Ranville, K. Tiede, Nanoparticle analysis and characterization methodologies in environmental risk assessment of engineered nanoparticles, Ecotoxicology. 17 (2008) 344–361, https://doi.org/10.1007/s10646-008-0225-x.

[17] F. Laborda, E. Bolea, J. Jiménez-Lamana, Single particle inductively coupled plasma mass spectrometry: a powerful tool for nanoanalysis, Anal. Chem. 86 (2014) 2270–2278, https://doi.org/10.1021/ac402980q.

[18] H.E. Pace, N.J. Rogers, C. Jarolimek, V.A. Coleman, C.P. Higgins, J.F. Ranville, Determining transport efficiency for the purpose of counting and sizing nanoparticles via single particle inductively coupled plasma mass spectrometry, Anal. Chem. 83 (2011) 9361–9369, https://doi.org/10.1021/ac201952t.

[19] D.M. Mitrano, E.K. Lesher, A. Bednar, J. Monserud, C.P. Higgins, J.F. Ranville, Detecting nanoparticulate silver using single-particle inductively coupled plasma-mass spectrometry, Environ. Toxicol. Chem. 31 (2012) 115–121, https://doi.org/10.1002/etc.719.

[20] F. Laborda, E. Bolea, J. Jiménez-Lamana, Single particle inductively coupled plasma mass spectrometry for the analysis of inorganic engineered nanoparticles in environmental samples, Trends Environ. Anal. Chem. 9 (2016) 15–23, https://doi.org/10.1016/j.teac.2016.02.001.

[21] F. Laborda, J. Jiménez-Lamana, E. Bolea, J.R. Castillo, Critical considerations for the determination of nanoparticle number concentrations, size and number size distributions by single particle ICP-MS, J. Anal. At. Spectrom. 28 (2013) 1220–1232, https://doi.org/10.1039/c3ja50100k.

[22] S. Lee, X. Bi, R.B. Reed, J.F. Ranville, P. Herckes, P. Westerhoff, Nanoparticle size detection limits by single particle ICP-MS for 40 elements, Environ. Sci. Technol. 48 (2014) 10291–10300, https://doi.org/10.1021/es502422v.

[23] J.W. Olesik, P.J. Gray, Considerations for measurement of individual nanoparticles or microparticles by ICP-MS: determination of the number of particles and the analyte mass in each particle, J. Anal. At. Spectrom. 27 (2012) 1143–1155, https://doi.org/10.1039/c2ja30073g.

[24] M.P. Dziewatkoski, L.B. Daniels, J.W. Olesik, Time-resolved inductively coupled plasma mass spectrometry measurements with individual, monodisperse drop sample introduction, Anal. Chem. 68 (1996) 1101–1109, https://doi.org/10.1021/ac951013b.

[25] K. Niemax, Considerations about the detection efficiency in inductively coupled plasma mass spectrometry, Spectrochim. Acta Part B At. Spectrosc. 76 (2012) 65–69, https://doi.org/10.1016/j.sab.2012.06.027.

[26] A. Murtazin, S. Groh, K. Niemax, Investigation of sample introduction- and plasma-related matrix effects in inductively coupled plasma spectrometry applying single analyte droplet and particle injection, Spectrochim. Acta Part B At. Spectrosc. 67 (2012) 3–16, https://doi.org/10.1016/j.sab.2011.12.003.

[27] S. Kaneco, T. Nomizu, T. Tanaka, N. Mizutani, H. Kawaguchi, Optimization of operating conditions in individual airborne particle analysis by inductively coupled plasma mass spectrometry, Anal. Sci. 11 (1995) 835–840, https://doi.org/10.2116/analsci.11.835.

[28] I. Kálomista, A. Kéri, G. Galbács, Optimization of plasma sampling depth and aerosol gas flow rates for single particle inductively coupled plasma mass spectrometry analysis 172, 2017, pp. 147–154, https://doi.org/10.1016/j.talanta.2017.05.051.

[29] K.S. Ho, W.W. Lee, W.T. Chan, Effects of ionization potential of an element and boiling point of the corresponding oxide on the sensitivity of ICP-MS, J. Anal. At. Spectrom. 30 (2015) 2066–2073, https://doi.org/10.1039/c5ja00137d.

[30] W.W. Lee, W.T. Chan, Calibration of single-particle inductively coupled plasma-mass spectrometry (SP-ICP-MS), J. Anal. At. Spectrom. 30 (2015) 1245–1254, https://doi.org/10.1039/c4ja00408f.

[31] K.S. Ho, K.O. Lui, K.H. Lee, W.T. Chan, Considerations of particle vaporization and analyte diffusion in single-particle inductively coupled plasma-mass spectrometry, Spectrochim. Acta Part B At. Spectrosc. 89 (2013) 30–39, https://doi.org/10.1016/j.sab.2013.08.012.

[32] F. Vanhaecke, R. Dams, C. Vandecasteele, "Zone model" as an explanation for signal behaviour and non-spectral interferences in inductively coupled plasma mass spectrometry, J. Anal. At. Spectrom. 8 (1993) 433–438, https://doi.org/10.1039/JA9930800433.

[33] C.C. Garcia, A. Murtazin, S. Groh, V. Horvatic, K. Niemax, Characterization of single Au and SiO2 nano- and microparticles by ICP-OES using monodisperse droplets of standard solutions for calibration, J. Anal. At. Spectrom. 25 (2010) 645–653, https://doi.org/10.1039/b921041e.

[34] M. Vaughan, G. Horlick, S.H. Tan, Effect of operating parameters on analyte signals in inductively coupled plasma mass spectrometry, J. Anal. At. Spectrom. 2 (1987) 765–772, https://doi.org/10.1039/JA9870200765.

[35] G. Zhu, R.F. Browner, Investigation of experimental parameters with a quadrupole ICP/MS, Appl. Spectrosc. 41 (1987) 349–359, https://doi.org/10.1366/0003702874448869.

[36] M. Aghaei, H. Lindner, A. Bogaerts, Optimization of operating parameters for inductively coupled plasma mass spectrometry: a computational study, Spectrochim. Acta Part B At. Spectrosc. 76 (2012) 56–64, https://doi.org/10.1016/j.sab.2012.06.006.

[37] A.L. Gray, J.G. Williams, System optimisation and the effect on polyatomic, oxide and doubly charged ion response of a commercial inductively coupled plasma mass spectrometry instrument, J. Anal. At. Spectrom. 2 (1987) 81–82, https://doi.org/10.1039/JA9870200081.

[38] D. Mozhayeva, C. Engelhard, A critical review of single particle inductively coupled plasma mass spectrometry – a step towards an ideal method for nanomaterial characterization, J. Anal. At. Spectrom. (2019), https://doi.org/10.1039/c9ja00206e.

[39] D.C. Montgomery, Design and Analysis of Experiments, 7th ed., Wiley, 2009.

[40] S.A. Weissman, N.G. Anderson, Design of Experiments (DoE) and Process Optimization. A Review of Recent Publications 19, Org. Process Res. Dev., 2015, pp. 1605–1633, https://doi.org/10.1021/op500169m.

[41] V. Geertsen, E. Barruet, F. Gobeaux, J.L. Lacour, O. Taché, Contribution to accurate spherical gold nanoparticle size determination by single-particle inductively coupled mass spectrometry: a comparison with small-angle X-ray scattering, Anal. Chem. 90 (2018) 9742–9750, https://doi.org/10.1021/acs.analchem.8b01167.

[42] M.D. Montaño, J.W. Olesik, A.G. Barber, K. Challis, J.F. Ranville, Single particle ICP-MS: advances toward routine analysis of nanomaterials, Anal. Bioanal. Chem. 408 (2016) 5053–5074, https://doi.org/10.1007/s00216-016-9676-8.

[43] J. Liu, K.E. Murphy, R.I. Maccuspie, M.R. Winchester, Capabilities of single particle inductively coupled plasma mass spectrometry for the size measurement of nanoparticles: a case study on gold nanoparticles, Anal. Chem. 86 (2014) 3405–3414, https://doi.org/10.1021/ac403775a.

[44] R.C. Merrifield, C. Stephan, J.R. Lead, Single-particle inductively coupled plasma mass spectroscopy analysis of size and number concentration in mixtures of monometallic and bimetallic (core-shell) nanoparticles, Talanta. 162 (2017) 130–134, https://doi.org/10.1016/j.talanta.2016.09.070.

[45] S. Gschwind, M.D.L. Aja Montes, D. Günther, Comparison of sp-ICP-MS and MDG-ICP-MS for the determination of particle number concentration, Anal. Bioanal. Chem. 407 (2015) 4035–4044, https://doi.org/10.1007/s00216-015-8620-7.

[46] M. Shivhare, G. McCreath, Practical considerations for DoE implementation in quality by design, Bioprocess Int. 8 (2010) 22–30.

[47] A. Bogaerts, M. Aghaei, Inductively coupled plasma-mass spectrometry: insights through computer modeling, J. Anal. At. Spectrom. 32 (2017) 233–261, https://doi.org/10.1039/c6ja00408c.

[48] H. Lindner, A. Murtazin, S. Groh, K. Niemax, A. Bogaerts, Simulation and experimental studies on plasma temperature, flow velocity, and injector diameter effects for an inductively coupled plasma, Anal. Chem. 83 (2011) 9260–9266, https://doi.org/10.1021/ac201699q.

[49] J. Fuchs, M. Aghaei, T.D. Schachel, M. Sperling, A. Bogaerts, U. Karst, Impact of the particle diameter on ion cloud formation from gold nanoparticles in ICPMS, Anal. Chem. 90 (2018) 10271–10278, https://doi.org/10.1021/acs.analchem.8b02007.

[50] S. Candás-Zapico, D.J. Kutscher, M. Montes-Bayón, J. Bettmer, Single particle analysis of TiO2 in candy products using triple quadrupole ICP-MS, Talanta. 180 (2018) 309–315, https://doi.org/10.1016/j.talanta.2017.12.041.
[51] J.G. Fernández, C. Sánchez-González, J. Bettmer, J. Llopis, N. Jakubowski, U. Panne, M. Montes-Bayón, Quantitative assessment of the metabolic products of iron oxide nanoparticles to be used as iron supplements in cell cultures, Anal. Chim. Acta 1039 (2018) 24–30, https://doi.org/10.1016/j.aca.2018.08.003.
[52] K. Newman, C. Metcalfe, J. Martin, H. Hintelmann, P. Shaw, A. Donard, Improved single particle ICP-MS characterization of silver nanoparticles at environmentally relevant concentrations, J. Anal. At. Spectrom. 31 (2016) 2069–2077. doi:https://doi.org/10.1039/c6ja00221h.
[53] S. Bazargan, R. Hill, H. Badiei, Systems and methods for automated analysis of output in single particle inductively coupled plasma mass spectrometry and similar data sets, US 9, 754,774 B2, 2017.
[54] O. Mestek, M. Loula, A. Kaňa, M. Vosmanská, Can ultrafast single-particle analysis using ICP-MS affect the detection limit? Case study: silver nanoparticles, Talanta. 210 (2020) 120665, https://doi.org/10.1016/j.talanta.2019.120665.
[55] J. Liu, K.E. Murphy, M.R. Winchester, V.A. Hackley, Overcoming challenges in single particle inductively coupled plasma mass spectrometry measurement of silver nanoparticles, Anal. Bioanal. Chem. 409 (2017) 6027–6039, https://doi.org/10.1007/s00216-017-0530-4.
[56] S. Groh, C.C. Garcia, A. Murtazin, V. Horvatic, K. Niemax, Local effects of atomizing analyte droplets on the plasma parameters of the inductively coupled plasma, Spectrochim. Acta Part B At. Spectrosc. 64 (2009) 247–254, https://doi.org/10.1016/j.sab.2009.02.008.
[57] M. Guillong, D. Günther, Effect of particle size distribution on ICP-induced elemental fractionation in laser ablation-inductively coupled plasma-mass spectrometry, J. Anal. At. Spectrom. 17 (2002) 831–837, https://doi.org/10.1039/b202988j.
[58] M. Loula, A. Kaňa, O. Mestek, Non-spectral interferences in single-particle ICP-MS analysis: an underestimated phenomenon, Talanta. 202 (2019) 565–571, https://doi.org/10.1016/j.talanta.2019.04.073.
[59] R. Peters, Z. Herrera-Rivera, A. Undas, M. Van Der Lee, H. Marvin, H. Bouwmeester, S. Weigel, Single particle ICP-MS combined with a data evaluation tool as a routine technique for the analysis of nanoparticles in complex matrices, J. Anal. At. Spectrom. 30 (2015) 1274–1285, https://doi.org/10.1039/c4ja00357h.